Preprints of the 10th IFAC International Symposium on Dynamics and Control of Process Systems
The International Federation of Automatic Control
December 18-20, 2013. Mumbai, India

Linear and Nonlinear State Estimation in the Czochralski Process ⋆

Parsa Rahmanpour * **John Atle Bones** ** **Morten Hovd** *** **Jan Tommy Gravdahl** ***

* *Dept. of Engineering Cybernetics, Norwegian Univ. of Science and Technology (NTNU), NO-7491 Trondheim, Norway.* (e-mail: parsa.rahmanpour@itk.ntnu.no).
** *SINTEF, Materials and Chemistry, Trondheim, Norway*
*** *Dept. of Engineering Cybernetics, (NTNU)*

Abstract: The Czochralski process is the only method used commercially for production of monocrystalline silicon for semiconductor and solar cell applications. This paper explores the use of mathematical modeling as an aid in estimation of system state variables in the standard Czochralski process. A state-space model of the process is presented, describing the dynamics of the crystal radius and meniscus height with crystal radius as measured output. For the purpose of estimating the actual crystal radius during growth, three types of state estimators are developed based on the state-space model; the Kalman filter, the extended Kalman filter and the unscented Kalman filter. It is found that the latter two provide highly accurate state estimates with excellent noise suppression.

1. INTRODUCTION

The Czochralski (Cz) method is one of the few crystal growth techniques where the lateral surface shaping is performed without any contact with container walls. The principle is based on melting the source material in a crucible, dipping a rotating seed crystal into the melt, and pulling it up slowly. As the seed comes in contact with the melt, the melt solidifies on the seed and takes on the same crystallographic orientation as the seed. The seed is then slowly withdrawn from the melt, and surface tension causes the formation of a meniscus which connects the crystal to the melt. As the crystal is withdrawn, the melt solidifies along the top of the meniscus, causing the crystal to grow. The surface along which the material solidifies is referred to as the (crystal-melt) *interface*. The finished crystal is called an *ingot*. The crystallization process can be described mathematically using the conservation of mass and the heat balance around the meniscus. Jan Czochralski discovered this method in the early 1900's, but it has only found wide practical application during the last decades because of the development of semiconductor engineering and the solar industries. After production of the ingot, it is cut into thin wafers, and each wafer cut into a specific shape (typically quadratic) depending on the final application.

This paper investigates and compares the performance of the Kalman filter, the Extended Kalman filter and the Unscented Kalman filter, based on a simulation study using a physically motivated model for the Czochralski process. Section 2 will give a brief introduction to the Czochralski process and present a simplified process model, section 3 will give a brief introduction to Kalman Filter (KF), Extended Kalman Filter (EKF) and Unscented Kalman Filter (UKF) and present the implemented estimation design methods used for the Czochralski diameter control problem. Section 4 presents the results of applying the designed estimators to the process model, whereas section 5 contains discussion and conclusions. Section 1, subsection 2.1 and some parts of 2.2 in this paper are based on [Rahmanpour and Hovd, 2012].

⋆ Supported by Prediktor AS and the Research Council of Norway.

2. THE CZOCHRALSKI CRYSTALLIZATION PROCESS AND A MODEL FOR THE CRYSTAL RADIUS

2.1 Czochralski Process Description

A sketch of the Czochralski process is shown in Figure 1.

The solid silicon put in a crucible. Electrical heaters are used both to melt the silicon, and to maintain an appropriate temperature trajectory throughout the crystallization process. A small crystal seed is put in contact with the molten silicon, and the crystal is produced by slowly pulling the seed out of the melt. Initially, the crystal diameter is increased quite quickly, whereas for most of the duration of the process it is desirable to keep the crystal diameter constant. A sketch of the region around the meniscus is shown in Figure 2.

2.2 A Crystal Formation Model for the Czochralski Process

The basic phenomena that need to be covered by a model for the Czochralski process are the *capillary problem* and the *thermal conditions*. From the theory of hydrostatics, the equilibrium shape of the liquid surface is described by the Laplace capillary equation [Tatarchenko, 1993]:

$$\frac{\sigma_{LV}}{R_1} + \frac{\sigma_{LV}}{R_2} + g\rho_L \tilde{z} = \text{const.} \quad (1)$$

where σ_{LV} is the liquid surface tension coefficient at the three-phase boundary, ρ_L denotes the liquid density, and

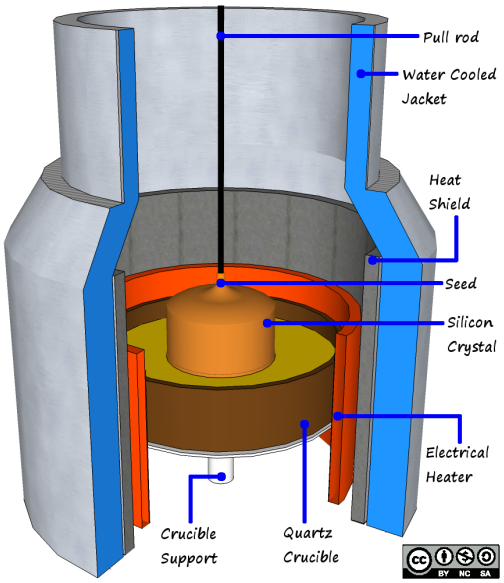

Fig. 1. An illustration of the main parts of the Czochralski crystallization process (This Figure is licensed under a Creative-Commons BY-NC-SA license).

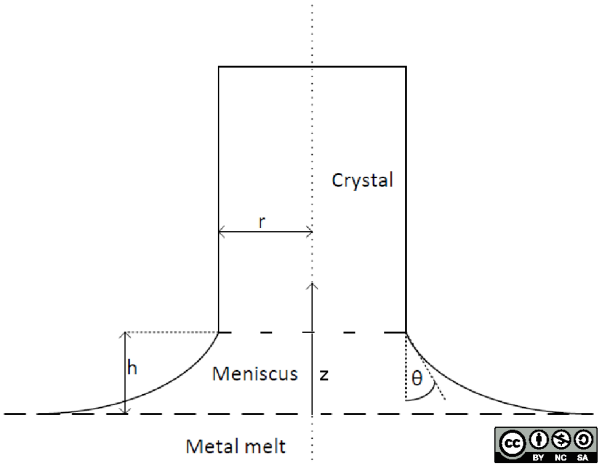

Fig. 2. A sketch of the crystal and its contact with the molten metal(This Figure is licensed under a Creative-Commons BY-NC-SA license).

R_1 and R_2 are the principal radii of curvature of the meniscus. The value of the constant is defined based on the selection of the origin of the $\tilde{z}$-coordinate and the difference between the pressure of the liquid p and gas p_v at the origin. With definition of the capillary constant $a = (2\sigma_{LV}/g\rho_L)^{1/2}$, we get a dimensionless coordinate $\tilde{z}/a = z$ where the $\tilde{z}$-axis is directed vertically upwards. The liquid surface meniscus for cylindrical or tubular crystals is obtained by rotating the profile curve around this axis. The shape of the free liquid surface is given by solution of the Laplace-Young equation [Tatarchenko, 1993]:

$$z^{''} r + z^{'}(1 + z^{'2}) \pm 2(d - z)(1 + z^{'2})^{3/2} = 0, \qquad d = \frac{p \cdot a}{2\sigma_{LV}} \tag{2}$$

Here z and r represent the vertical and radial coordinates, while a is the Laplace constant. For the thermal part of the model, much research has been devoted to calculation of the temperature field in the crystal-melt system. However, because of the variety of growth configurations and the presence of a great number of elements that must be considered while studying the thermal conductivity problems, a complete mathematical description of heat transfer throughout the process is extremely difficult. Analytical solutions are usually achieved by applying many simplifications [Tatarchenko, 1993].

A heat transfer balance about the interface states that the heat flow caused by crystallization (Φ_h) is given by the difference between the heat flow from the interface to the crystal (Φ_s) and the heat flow from the melt to the interface (Φ_l) [Winkler et al., 2010, pp. 1007,1012]:

$$\Phi_h = \Phi_s - \Phi_l \tag{3}$$

where

$$\Phi_h = \rho_s v_g A_i \Delta H \tag{4a}$$
$$\Phi_s = k_s A_i \nabla T_s \tag{4b}$$
$$\Phi_l = k_l A_i \nabla T_l \tag{4c}$$

Here T_s and T_l denote the temperatures in the solid and the melt, respectively, ρ_s is solid state density, k_s and k_l are the thermal conductivity coefficients in crystal and the melt, ΔH is the latent heat of fusion per unit volume, v_g is the growth velocity normal to the interface along with the pulling direction, and A_i is the interface or meniscus area. An accurate model for the Czochralski process will necessarily result in a highly complex model involving coupled PDE's [Tatarchenko, 1993]. Such simulation models do exist, but they are typically based on assuming quasi-stationarity conditions and are anyway too complex for controller design.

Steel and Hill [1975, p. 49] and Hurle et al. [1990, p. 15] suggest the following estimate of the melt temperature gradient under the assumption that the heat radiation from the meniscus to the environment is negligible

$$\nabla T_l \approx \frac{T_B - T_M}{h} \tag{5}$$

This results in the following expression for the melt-meniscus heat flow

$$\Phi_l \approx k_l A_i \frac{T_B - T_M}{h} \tag{6}$$

Here T_B is the temperature at the base of the meniscus, T_M is the melting temperature (at the lower surface of the cylindrical crystal). Since, over time, the growth rate (v_g) equals the average pulling rate (v_p), the following estimate of the rate of heat release can be obtained from (4a) by assuming a flat interface:

$$\Phi_h \approx \pi r_c^2 \rho_s \Delta H v_p \tag{7}$$

In describing the dynamics of the crystal radius, the growth rate is the most important quantity. It can be calculated from the heat flow caused by crystallization (4a) as follows

$$v_g = \frac{\Phi_h}{\pi r_c^2 \rho_s \Delta H} \tag{8a}$$

where a flat interface has been assumed. By considering (3), (4b), (6) and (8a), the following expression for the growth rate is obtained

$$v_{\mathrm{g}} = \frac{1}{\rho_{\mathrm{s}} \Delta H} \left(k_{\mathrm{s}} \Delta T_{\mathrm{s}} - \frac{k_{\mathrm{l}}}{h} (T_{\mathrm{B}} - T_{\mathrm{M}}) \right) \tag{9}$$

where ΔT_{s} represents the temperature gradient in the crystal.

During growth, the radius (diameter) of the crystal is typically measured by a CCD camera aimed at the meniscus. In such an approach, the height above the liquid surface where the camera is focused at is denoted z_{CCD} and $r_{\mathrm{m}}(z_{\mathrm{CCD}})$ is the deviation from the actual meniscus radius, found trough Hurle's analytical expression for the meniscus shape [Duffar, 2010, p. 475]. A mathematical description of the measured radius can be useful in determining the true radius based on the measurement. During stationary growth, this contribution is given by $r_{\mathrm{m},0}$. The measured radius can now be written as

$$r_{\mathrm{CCD}} = r_{\mathrm{c}} + r_{\mathrm{m}}(z_{\mathrm{CCD}}) - r_{\mathrm{m},0} \tag{10}$$

Here, the stationary contribution of the meniscus has been subtracted to give a radius measurement as close as possible to the true radius.

Preferably, the estimators should estimate both states (r_{c}, h). Since the radius (r_{c}) is the only quantity that is measured (r_{CCD}), it will allow the estimators to correct their estimates based on radius measurement. For the case of the meniscus height (h), there exists no such measurement to be used for correction of estimates. Two types of additive noise models have been applied to the nonlinear system; low-pass filtered white noise on v_{g}, and white noise on r_{CCD}. The first one represents model uncertainty (melt turbulence), while the latter acts as measurement noise.

Assuming that the vertical position of the melt level is kept constant, which means that the crucible lift rate is such that it compensates for the drop in melt level, leaves the following simple model [Hurle et al., 1989]:

$$\dot{\mathbf{x}} = \mathbf{f}(\mathbf{x}, \mathbf{u}) \tag{11a}$$
$$y = g(\mathbf{x}) \tag{11b}$$

with

$$\mathbf{f}(\mathbf{x}, u) = [f_1, f_2]^\top = [v_{\mathrm{g}} \tan\theta, v_{\mathrm{p}} - v_{\mathrm{g}}]^\top \tag{12a}$$
$$g(\mathbf{x}) = r_{\mathrm{CCD}}, \quad \mathbf{x} = [r_{\mathrm{c}}, h]^\top, \quad u = v_{\mathrm{p}} \tag{12b}$$

where θ defines the growth angle. For most of the crystal, the growth angle θ is small and nearly constant, but it cannot be measured during operation. Instead we replace it with the approximation [Duffar, 2010].

$$\sin(\theta) \approx 1 - \left(\frac{h}{a}\right)^2 \left(1 + \frac{a}{r\sqrt{2}}\right) \approx \theta \tag{13}$$

Here a, as above, represents the Laplace constant. In normal operation, the angle θ will stay within a few degrees from zero. Thus, we can use the approximation $\tan(\theta) \approx \sin(\theta) \approx \theta$ for $\theta \approx 0$.

Linearized system dynamics The KF and the EKF require a linear model. Through Taylor series expansion of these equations, a standard LTI model is obtained

$$\dot{\bar{\mathbf{x}}} = \mathbf{A}\bar{\mathbf{x}} + \mathbf{B}\bar{u} + \mathbf{E}\bar{\mathbf{w}} \tag{14a}$$
$$\bar{y} = \mathbf{C}\bar{\mathbf{x}} + D\bar{u} + H\bar{v} \tag{14b}$$

with

$$\bar{\mathbf{w}} = \mathbf{w} - \mathbf{w}_0 = \mathbf{w} = [w_1, w_2]^\top = [0, v_{\mathrm{g,noise}}]^\top \tag{15a}$$
$$\bar{v} = v - v_0 = v \tag{15b}$$

where

$$\mathbf{A} = \left[\begin{matrix} \frac{\partial f_1}{\partial r_{\mathrm{c}}} & \frac{\partial f_1}{\partial h} \\ \frac{\partial f_2}{\partial r_{\mathrm{c}}} & \frac{\partial f_2}{\partial h} \end{matrix}\right]\Bigg|_* = \left[\begin{matrix} v_{\mathrm{g},0} \left.\frac{\partial \theta}{\partial r_{\mathrm{c}}}\right|_* & v_{\mathrm{g},0} \left.\frac{\partial \theta}{\partial h}\right|_* \\ 0 & 0 \end{matrix}\right]$$
$$\approx \begin{bmatrix} 0 & -2\frac{h_0}{a} v_{\mathrm{g},0} \\ 0 & 0 \end{bmatrix} \tag{16a}$$

$$\mathbf{B} = \left[\frac{\partial f_1}{\partial u}, \frac{\partial f_2}{\partial u}\right]^\top\Bigg|_* = [0, 1]^\top \tag{16b}$$

$$\mathbf{C} = \left[\frac{\partial g}{\partial r_{\mathrm{c}}} \; \frac{\partial g}{\partial h}\right]\Bigg|_* = \left[\frac{\partial r_{\mathrm{CCD}}}{\partial r_{\mathrm{c}}} \; \frac{\partial r_{\mathrm{CCD}}}{\partial h}\right]\Bigg|_*$$
$$\approx \left[1, \left.\frac{\partial r_{\mathrm{CCD}}}{\partial h}\right|_*\right] \tag{16c}$$

$$\mathbf{D} = \left.\frac{\partial g}{\partial u}\right|_* = 0 \tag{16d}$$

$$\mathbf{E} = \left[\frac{\partial f_1}{\partial w_1}, \frac{\partial f_2}{\partial w_2}\right]^\top\Bigg|_* = \begin{bmatrix} 0 \\ -1 \end{bmatrix} \tag{16e}$$

$$\mathbf{H} = \left.\frac{\partial g}{\partial v}\right|_* = 1 \tag{16f}$$

and where $*$ indicates the points at which the expressions are evaluated, i.e., the linearization points. With these matrices, the observability and controllability matrices are respectively given by

$$\mathcal{O} \approx \begin{bmatrix} 1 & \left.\frac{\partial r_{\mathrm{CCD}}}{\partial h}\right|_* \\ 0 & -2\frac{h_0}{a} v_{\mathrm{g},0} \end{bmatrix}, \quad \mathcal{C} \approx \begin{bmatrix} 0 & -2\frac{h_0}{a} v_{\mathrm{g},0} \\ 1 & 0 \end{bmatrix} \tag{17}$$

Both matrices have full rank, but the observability matrix has full rank for a positive growth rate, meaning that the system is structurally always observable, since $\partial r_{\mathrm{CCD}}/\partial h$ is always positive. This has been shown numerically in [Bones and Haugen, 2012].

3. STATE ESTIMATION

The meniscus height is not measurable and the measured radius is quite noisy. Thus, the actual radius and the meniscus height are not available during crystal growth. Therefore, use of feedback from estimators that attempt to compute these quantities are explored. Three types of state estimators are investigated: the Kalman filter, the extended Kalman filter and the unscented Kalman filter. With the exception of the latter, these estimators all contain a linear model and use the measured radius as an input to correct their estimates. It is common to convert the continuous-time model (f, g) to a discrete-time model (F, G) in order to implement the model in a computer. Therefore, the estimator equations in this

section are illustrated in their discrete-time version. The following notation is used in this section:

- $\bar{\mathbf{x}}$ is the mean value of $\mathbf{x}$
- $\hat{\mathbf{x}}$ is the state estimate
- $\hat{\mathbf{x}}^-$ is the predicted (a priori) state estimate
- $\hat{\mathbf{y}}$ is the measurement estimate
- $\mathbf{P}$ is the estimate covariance
- $\mathbf{Q}$ is the covariance of the process noise
- $\mathbf{R}$ is the covariance of the observation noise
- $\mathbf{K}_k$ is the Kalman gain

3.1 Kalman Filter Design

The Kalman filter (KF) assumes that the process is linear and can be modeled on the following form

$$\mathbf{x}_{k+1} = \mathbf{A}_{\mathrm{d},k}\mathbf{x}_k + \mathbf{B}_{\mathrm{d},k}\mathbf{u}_k + \mathbf{E}_{\mathrm{d},k}\mathbf{w}_k$$
$$\mathbf{y}_k = \mathbf{C}_{\mathrm{d},k}\mathbf{x}_k + \mathbf{H}_{\mathrm{d},k}\mathbf{v}_k$$

where the noise vectors $\mathbf{w}$ and $\mathbf{v}$ are white noise with zero mean. Its estimates are *optimal* in the case that the model is perfect, the noise is white and the covariances of the noise are known. That is, optimal in the sense that it minimizes the mean of the squared estimate error. For more information on KF see [Brown and Hwang, 1997].

- **Step 1: Predict**

  Predict new state estimate at time $k+1$ based on information available at time k

  $$\hat{\mathbf{x}}^-_{k+1} = \mathbf{A}_{\mathrm{d},k}\hat{\mathbf{x}}_k + \mathbf{B}_{\mathrm{d},k}\mathbf{u}_k$$

  Compute the error covariance of the new estimate

  $$\mathbf{P}^-_{k+1} = \mathbf{A}_{\mathrm{d},k}\mathbf{P}_k\mathbf{A}^\top_{\mathrm{d},k} + \mathbf{E}_{\mathrm{d},k}\mathbf{Q}_k\mathbf{E}^\top_{\mathrm{d},k}$$

- **Step 2: Update**

  Compute the Kalman gain

  $$\mathbf{K}_k = \mathbf{P}^-_k\mathbf{C}^\top_{\mathrm{d},k}\left(\mathbf{C}_{\mathrm{d},k}\mathbf{P}^-_k\mathbf{C}^\top_{\mathrm{d}} + \mathbf{R}_{\mathrm{d},k}\right)^{-1}$$

  Update the state estimates

  $$\hat{\mathbf{y}}_k = \mathbf{C}_{\mathrm{d},k}\hat{\mathbf{x}}^-_k$$
  $$\hat{\mathbf{x}}_k = \hat{\mathbf{x}}^-_k + \mathbf{K}_k\left(\mathbf{y}_k - \hat{\mathbf{y}}_k\right)$$

  Compute the error covariance for the updated estimate

  $$\mathbf{P}_k = \mathrm{E}\left[\mathbf{e}_k\mathbf{e}^\top_k\right]$$
  $$= \left(\mathbf{I} - \mathbf{K}_k\mathbf{C}_{\mathrm{d},k}\right)\mathbf{P}^-_k\left(\mathbf{I} - \mathbf{K}_k\mathbf{C}_{\mathrm{d}}\right)^\top + \mathbf{K}_k\mathbf{R}_{\mathrm{d},k}\mathbf{K}^\top_k$$

3.2 Extended Kalman Filter Design

In an attempt to further enhance the estimation accuracy, simulations have also been carried out using an *Extended Kalman Filter* (*EKF*). The EKF is quite similar in structure to the linear version. The main differences are that the extended Kalman filter uses a nonlinear model to predict a new state estimate, and that the linear model used for updating the estimates is re-linearized along the systems trajectories. In this case, the algorithm takes the following form [Brown and Hwang, 1997, pp. 343-347]

- **Step 1: Predict**

  Predict new state estimate

  $$\hat{\mathbf{x}}^-_{k+1} = \mathbf{F}(\hat{\mathbf{x}}_k, \mathbf{u}_k)$$

  Compute the error covariance of the new estimate

  $$\mathbf{P}^-_{k+1} = \mathbf{A}_{\mathrm{d},k}\mathbf{P}_k\mathbf{A}^\top_{\mathrm{d},k} + \mathbf{E}_{\mathrm{d},k}\mathbf{Q}_k\mathbf{E}^\top_{\mathrm{d},k}$$

- **Step 2: Update**

  Compute the Kalman gain

  $$\mathbf{K}_k = \mathbf{P}^-_k\mathbf{C}^\top_{\mathrm{d},k}\left(\mathbf{C}_{\mathrm{d},k}\mathbf{P}^-_k\mathbf{C}^\top_{\mathrm{d}} + \mathbf{R}_{\mathrm{d},k}\right)^{-1}$$

  Update the state estimates

  $$\hat{\mathbf{x}}_k = \hat{\mathbf{x}}^-_k + \mathbf{K}_k\left[\mathbf{y}_k - \mathbf{G}\left(\hat{\mathbf{x}}^-_k, \mathbf{u}_k, k\right)\right]$$

  Compute the error covariance for the updated estimate

  $$\mathbf{P}_k = \mathrm{E}\left[\mathbf{e}_k\mathbf{e}^\top_k\right]$$
  $$= \left(\mathbf{I} - \mathbf{K}_k\mathbf{C}_{\mathrm{d},k}\right)\mathbf{P}^-_k\left(\mathbf{I} - \mathbf{K}_k\mathbf{C}_{\mathrm{d}}\right)^\top + \mathbf{K}_k\mathbf{R}_{\mathrm{d},k}\mathbf{K}^\top_k$$

where the Jacobian matrices $\mathbf{A}_{\mathrm{d},k}$ and $\mathbf{C}_{\mathrm{d},k}$ are re-calculated along the systems trajectories according to the discretization of

$$\mathbf{A}_{\mathrm{d},k} = \left.\frac{\partial \mathbf{f}}{\partial \mathbf{x}}\right|_{\hat{\mathbf{x}}_k, \mathbf{u}_k} \quad \text{and} \quad \mathbf{C}_{\mathrm{d},k+1} = \left.\frac{\partial g}{\partial \mathbf{x}}\right|_{\hat{\mathbf{x}}^-_{k+1}, \mathbf{u}_k}$$

3.3 Unscented Kalman Filter Design

The basic idea behind extension of Kalman filter to unscented Kalman filter can be formulated simply by the following statement: "We use the intuition that it is easier to approximate a probability distribution than it is to approximate an arbitrary nonlinear function of transformation [Julier and Uhlmann, 2004]."

Although the extended Kalman filter (EKF) is the most widely applied state estimation algorithm for nonlinear systems, it can, however, be difficult and exhausting to tune and often gives unreliable estimates if the system nonlinearities are severe [Simon, 2006]. This is because in EKF, propagation of the mean and covariance of the state relies on linearization. Due to the complex and nonlinear system dynamics in this case, the unscented Kalman filter (UKF), as an alternative extension of the Kalman filter, is used. This is because UKF reduces the linearization error of the EKF and can provide significant improvements over the EKF [Simon, 2006].

In UKF, the state distribution is represented by a Gaussian random variable (GRV) which is specified using a minimal set of carefully chosen sample points (*sigma points*). These sample points completely capture the true mean and covariance of the GRV, and when propagated through the true nonlinear system dynamics, capture the posterior mean and covariance accurately to the second order (Taylor series expansion) for any nonlinearity. The statistics of the transformed points can then be calculated to form an estimate of the nonlinearly transformed mean and covariance [Haykin, 2001].

It is noticeable that the sigma points are not chosen randomly; they are deterministically chosen so that they exhibit certain properties. Furthermore, the sigma points can be weighted [Julier and Uhlmann, 2004]. Assume propagating a random variable x of dimension L through $\mathbf{y} = \mathbf{f}(\mathbf{x})$ with mean and covariance defined above. To calculate the statistics of the propagated points ($\mathbf{y}$), a matrix χ of $2L+1$ sigma vectors χ_i is defined as [Haykin, 2001]:

$$\begin{aligned}
\chi_0 &= \bar{\mathbf{x}}, \\
\chi_i &= \bar{\mathbf{x}} + (\sqrt{(L+\lambda)\mathbf{P}_{\mathbf{x}}})_i, \quad i = 1, \cdots, L \\
\chi_i &= \bar{\mathbf{x}} - (\sqrt{(L+\lambda)\mathbf{P}_{\mathbf{x}}})_{i-L}, \; i = L+1, \cdots, 2L
\end{aligned} \tag{21}$$

where $\lambda = \alpha^2(L+\kappa) - L$ is a scaling parameter. The constant α determines the spread of the sigma points around $\bar{\mathbf{x}}$, and is usually small ($1 \geq \alpha \geq 10^{-4}$). κ and β are also scaling parameters. $(\sqrt{(L+\lambda)\mathbf{P_x}})_i$ is the ith column of the lower-triangular Cholesky factorization. The UKF used in this paper is implemented as described in [Haykin, 2001], where a full description of how to select scaling parameters also can be found. The weights applied to the propagated sigma points are defined as follows:

$$\begin{aligned} W_0^{(m)} &= \frac{\lambda}{L+\lambda}, \\ W_0^{(c)} &= \frac{\lambda}{L+\lambda} + 1 - \alpha^2 + \beta, \\ W_i^{(m)} &= W_i^{(c)} = \frac{1}{2(L+\lambda)}, \quad i = 1, \cdots, 2L \end{aligned} \tag{22}$$

These sigma vectors are propageted through the nonlinear dynamics to obtain for each sigma vector χ_i a predicted next timestep state $\chi^*_{k|k-1}$. These predicted next timestep states are used to find both the *a priori* next step state estimate $\hat{x}_k^-$ and the corresponding *a priori* state covariance estimate P_k^- (see step 2 below). Using these new *a priori* state and state covariance estimates, new sigma points are drawn around $\hat{x}_k^-$ and passed through the measurement function $g(x)$ to find a corresponding measurement for each of these new sigma points. These are used both to calculate the measurement covariance $P_{y_k y_k}$ and the cross covariance between state and measurement $P_{x_k y_k}$ (see step 3 below). With these covariance estimates, the UKF gain K_k and the *a posteriori* state covariance P_k follow from the same equations as for the ordinary discrete-time Kalman filter.

- **Step 1: Initialize**

  Initialize with

  $$\begin{aligned} \hat{\mathbf{x}}_0 &= \mathbb{E}[\mathbf{x_0}], \\ \mathbf{P_0} &= \mathbb{E}[(\mathbf{x_0} - \hat{\mathbf{x}}_0)(\mathbf{x_0} - \hat{\mathbf{x}}_0)^\top]. \end{aligned}$$

  For $k \in \{1, \cdots, \infty\}$, calculate the sigma points:

  $$\boldsymbol{\chi}_{k-1} = [\hat{\mathbf{x}}_{k-1} \quad \hat{\mathbf{x}}_{k-1} + \gamma\sqrt{\mathbf{P_{k-1}}} \quad \hat{\mathbf{x}}_{k-1} - \gamma\sqrt{\mathbf{P_{k-1}}}].$$

- **Step 2: Predict**

  The time-update equations are

  $$\begin{aligned} \boldsymbol{\chi}^*_{k|k-1} &= \mathbf{F}(\boldsymbol{\chi}_{\mathbf{k-1}}, \mathbf{u_{k-1}}) \\ \hat{\mathbf{x}}_k^- &= \sum_{i=0}^{2L} W_i^{(m)} \chi^*_{i,k|k-1} \\ \mathbf{P}_k^- &= \\ &\sum_{i=0}^{2L} W_i^{(c)} (\chi^*_{i,k|k-1} - \hat{\mathbf{x}}_k^-)(\chi^*_{i,k|k-1} - \hat{\mathbf{x}}_k^-)^\top + \mathbf{Q} \end{aligned}$$

- **Step 3: Update**

  We redraw a complete new set of sigma points

  $$\begin{aligned} \boldsymbol{\chi}_{k|k-1} &= [\hat{\mathbf{x}}_k^- \quad \hat{\mathbf{x}}_k^- + \gamma\sqrt{\mathbf{P_k^-}} \quad \hat{\mathbf{x}}_k^- - \gamma\sqrt{\mathbf{P_k^-}}] \\ \boldsymbol{\mathcal{Y}}_{k|k-1} &= \mathbf{G}(\boldsymbol{\chi}_{\mathbf{k|k-1}}) \\ \hat{\mathbf{y}}_\mathbf{k}^- &= \sum_{i=0}^{2L} W_i^{(m)} \mathcal{Y}_{i,k|k-1} \end{aligned}$$

  and the measurements-update equations are

$$\begin{aligned} &\mathbf{P}_{\mathbf{y_k y_k}} = \\ &\sum_{i=0}^{2L} W_i^{(c)} (\mathcal{Y}_{i,k|k-1} - \hat{\mathbf{y}}_\mathbf{k}^-)(\mathcal{Y}_{\mathbf{i,k|k-1}} - \hat{\mathbf{y}}_\mathbf{k}^-)^\top + \mathbf{R} \\ &\mathbf{P}_{\mathbf{x_k y_k}} = \\ &\sum_{i=0}^{2L} W_i^{(c)} (\chi_{i,k|k-1} - \hat{\mathbf{x}}_\mathbf{k}^-)(\mathcal{Y}_{\mathbf{i,k|k-1}} - \hat{\mathbf{y}}_\mathbf{k}^-)^\top \\ &\mathbf{K}_k = \mathbf{P}_{\mathbf{x_k y_k}} \mathbf{P}^{-1}_{\mathbf{y_k y_k}} \\ &\hat{\mathbf{x}}_k = \hat{\mathbf{x}}_k^- + \mathbf{K}_k(\mathbf{y_k} - \hat{\mathbf{y}}_\mathbf{k}^-) \\ &\mathbf{P_k} = \mathbf{P_k^-} - \mathbf{K_k} \mathbf{P}_{\mathbf{y_k y_k}} \mathbf{K_k^\top} \end{aligned}$$

where $\gamma = \sqrt{L+\lambda}$ and W_i are the weights as calculated in (22).

4. SIMULATION RESULTS

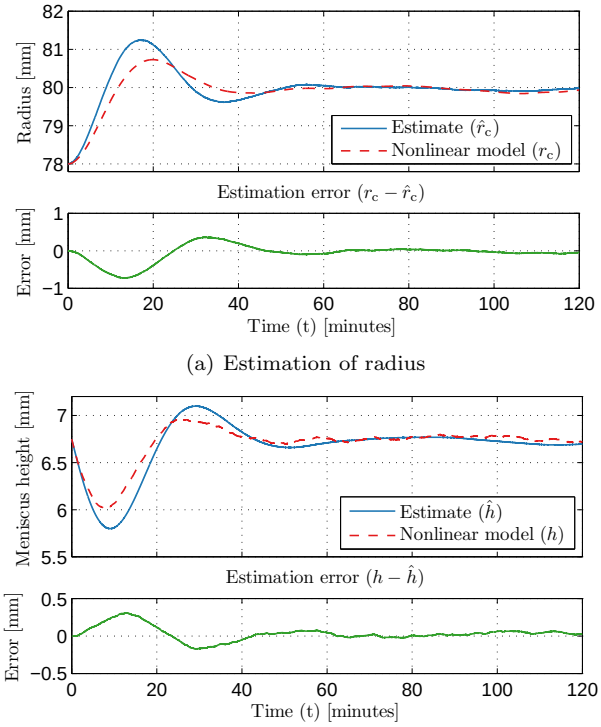

(a) Estimation of radius

(b) Estimation of meniscus height

Fig. 3. Estimation performance by Kalman Filter.

Figure 3(a) shows the estimated and actual radius in the first simulation case with KF, while Figure 3(b) compares the estimated meniscus height and what the nonlinear model expected. It is evident that the KF provides a good estimate in terms of noise reduction. However, since the process is nonlinear, it would still be possible to improve the accuracy of the estimate by using a nonlinear model for prediction of the states. Figure 4 illustrates also the estimated r_c and h. Clearly, the EKF yields a better result in terms of estimation error when compared to the KF. The simulation of the UKF is shown in Figure 5. The performance is about the same as that of the EKF, which may indicate that the nonlinearity is not strong enough to benefit very much from using the UKF. However, it should be noted that the adjustment of the tuning parameters (α, β, κ) might result in better estimates. Since the EKF and UKF provide highly accurate estimates and suppress

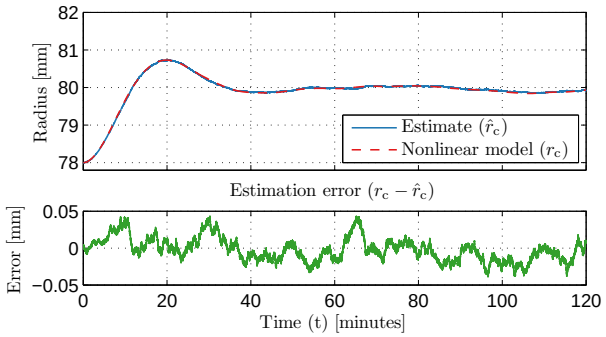

(a) Estimation of radius

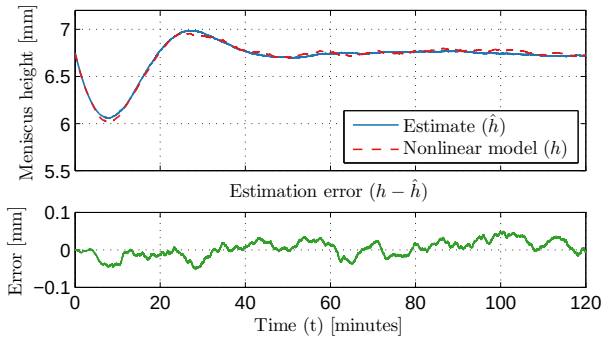

(b) Estimation of meniscus height

Fig. 4. Estimation performance by Extended Kalman Filter.

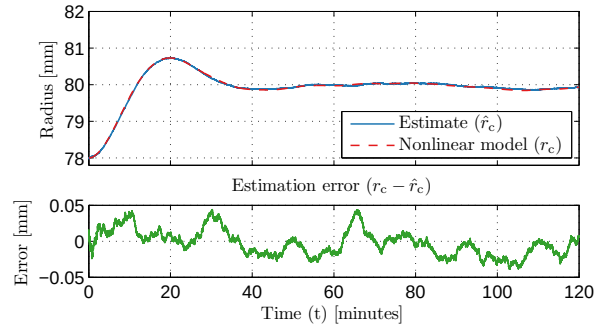

(a) Estimation of radius

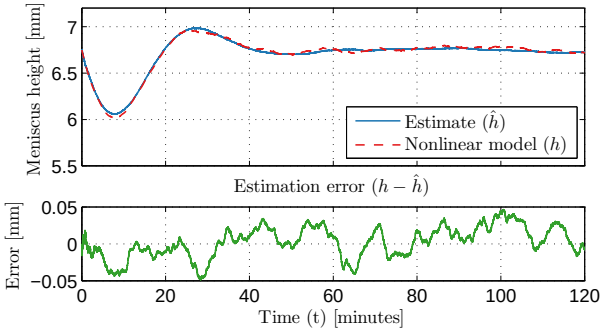

(b) Estimation of meniscus height

Fig. 5. Estimation performance by Unscented Kalman Filter.

noise very well, they will allow any applied controller to have higher bandwidth, when using the estimated states as feedback.

Table 1. Root Mean Square Error of estimates

Observers	RMSE of $\hat{r}_c$	RMSE of $\hat{h}$
KF	0.2404	0.1003
EKF	0.0159	0.0216
UKF	0.0178	0.0208

The overall performance of the estimators have been summarized in Table 1.

5. DISCUSSION AND CONCLUSIONS

It has been shown in this paper that the Kalman filters do an excellent job in dealing with measurement noise and provide acceptable estimates of both states, specially EKF and UKF. By using the estimate of the meniscus height and the actual radius rather than the measured radius as feedback in the conventional control scheme, better control of the radius should be achievable. Plans for future work include experimental verification of the simulation results.

REFERENCES

John Atle Bones and Kristian Haugen. Model-based control of the Czochralski Process. Master's thesis, Norwegian University of Science and Technology, 2012.

Robert G. Brown and Patrick Y. C. Hwang. *Introduction to Random Signals and Applied Kalman Filtering*. John Wiley & Sons, third edition, 1997.

Thierry Duffar. *Crystal Growth Processes Based on Capillarity: Czochralski, floating zone, shaping and techniques*. John Wiley & Sons, 2010.

Simon Haykin. *Kalman Filtering and Neural Networks*. John Wiley & Sons, 2001.

D.J. Hurle, G.C. Joyce, M. Ghassempoory, A.B. Crowley, and E.J. Stern. The dynamics of Czochralski Growth. *Journal of Crystal Growth*, 100:11–25, 1989.

D.T.J. Hurle, G.C. Joyce, M. Ghassempoory, A.B. Crowley, and E.J. Stern. The dynamics of Czochralski growth. *Journal of Crystal Growth*, 100(1-2): 11–25, 1990. ISSN 0022-0248. doi: 10.1016/0022-0248(90)90603-I.

S. Julier and J. Uhlmann. Unscented filtering and nonlinear estimation. *Proceedings of the IEEE*, 92(3), 2004.

Parsa Rahmanpour and Morten Hovd. Numerical backstepping for diameter control of silicon ingots in the Czochralski Process. 2012. Accepted to 51st IEEE Conference on Decision and Control, Maui, Hawaii.

D. J. Simon. *Optimal State Estimation*. John Wiley & Sons, 2006.

G.K. Steel and M.J. Hill. Analysis of the transfer function governing crystal growth in the Czochralski Process. *Journal of Crystal Growth*, 30(1):45 – 53, 1975. ISSN 0022-0248. doi: 10.1016/0022-0248(75)90198-0.

Y.A. Tatarchenko. *Shaped Crystal Growth*. Kluwer Academic Publishers, 1993.

J. Winkler, M. Neubert, and J. Rudolph. Nonlinear model-based control of the Czochralski process I: Motivation, modeling and feedback controller design. *Journal of Crystal Growth*, 312(7):1005–1018, 2010. ISSN 0022-0248. doi: 10.1016/j.jcrysgro.2009.12.074.